SLAC RADIATION PHYSICS NOTE **RP-05-02**
January 28, 2005

Streaming calculations through LCLS injector penetrations using MARS14 Monte Carlo code and comparison with analytical methods

Noriaki Nakao, Heinz Vincke and Stan Mao
Radiation Protection Department, MS-48
Stanford Linear Accelerator Center (SLAC)
P.O.Box 20450, Stanford, CA 94309

1) Introduction

Dose rate distributions through penetrations at the klystron gallery floor due to the beam loss of the LCLS injector were calculated using the MARS14 Monte Carlo code [1]. The results were compared with the FLUKA Monte Carlo code [2,3] in some case, and they agreed well. The maximum dose rates during operation in each penetration exit in the klystron gallery floor were estimated considering dark current.

The analytical calculations were also performed and compared with the MARS14 calculation results. The comparisons generally show agreements in factors, however, big disagreements of more than 2 orders of magnitude were found in the case of the target near the penetration mouth.

2) Operation parameters

The LCLS Injector is located at the off-axis housing at Sector 20 and consists of a photocathode RF gun followed by two SLAC accelerator sections. The nominal beam powers and the corresponding source locations are given in Table 1. Figs. 1 and 2 give the locations of the radiation sources due to the beam being stopped by various intercepting diagnostics.

In addition to the photocurrent beam, there is also a contribution from dark current (field emission) both in the gun and the accelerator sections. Nearly all the gun dark current is lost in the gun-to-linac region and therefore is not included in the high energy estimate. The linac dark current was determined to be 0.019 microamps for each structure [4] and for the worse case it is assumed that this beam is accelerated through both structures. After L0-1 there is the possibility of 0.019 microamps*(62-6.2)MeV = 1.06 watts due to L0-1 linac dark current. Similarly L0-2 could produce another 0.019*(135-62)=1.39 watts due to the dark current plus 0.019 microamps*(135-6.2)MeV = 2.45 watts due to acceleration of the dark current from L0-1. Thus if there is no loss of the L0-1 dark current, there will be two-components to the dark current energy spectrum after L0-2. Table 2 summarizes the dark current parameters for the injector.

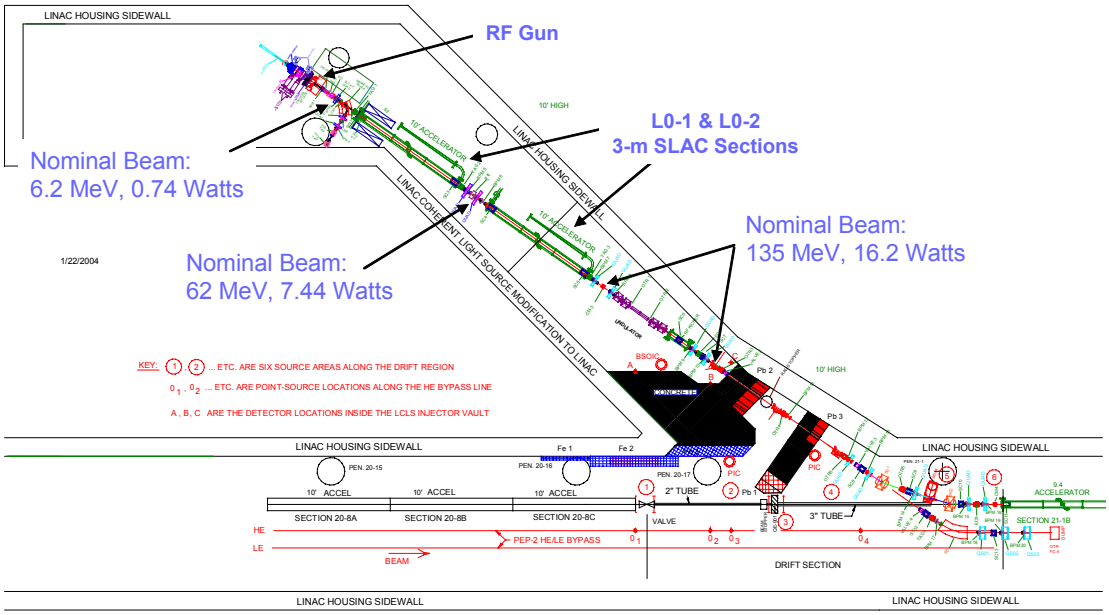

Fig. 1: Location of nominal beam radiation sources.

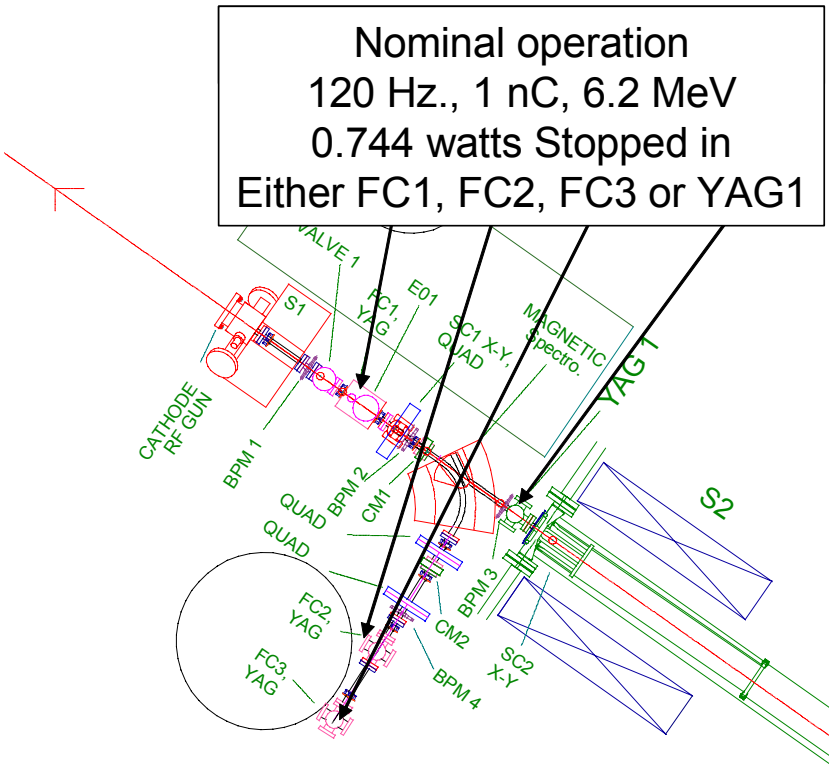

Fig. 2: Detail of source locations in the Gun-to-Linac region.

Table 1: Nominal operating parameters for the LCLS Injector.

	Nominal Energy (MeV)	Charge/Pulse (nC)	Current at 120 Hz (microamps)	Average Beam Power (Watts)
Gun-to-Linac	6.2	1nC	0.12	0.744
L0-1 to L0-2	62	1nC	0.12	7.44
After L0-2	135	1nC	0.12	16.2

Table 2: Dark Current for the LCLS Injector

	Dark Current Energy (MeV)	Dark Current Charge/Pulse (nC)	Current at 120 Hz (microamps)	Average Beam Power (Watts)
Gun-to-Linac	6.2	1	0.12	0.744
L0-1 to L0-2	55.8	0.158	0.019	1.06
After L0-2	73 128.8	0.158 0.316	0.019@73MeV 0.019@128.8MeV	1.39 2.45

3) Locations of beam losses and penetrations

Fig. 3 shows locations and names of six beam loss points labeled A~F. The electron beam loss is at A~D is 6.2 MeV, at E 62 MeV, and at F 135 MeV.

Four penetrations (1~4) and the stairway are also shown in Fig. 3. These penetrations reach the klystron gallery floor (ground level), and the distance from the ceiling of beam line tunnel is 25 ft (762 cm). Only penetration-3 has two bent section and the others are straight up to the gallery.

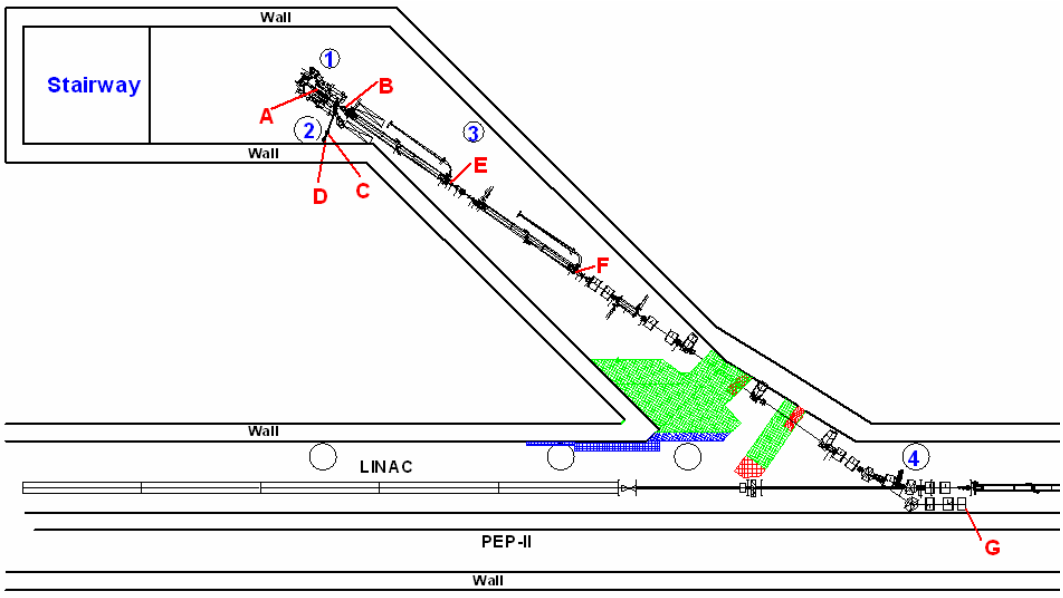

Fig. 3: Locations and names of penetrations and beam loss points.

4) MARS14 Monte Carlo Calculation

Calculations using the MARS14 Monte Carlo code [1] were performed to estimate dose rates at the penetration exits at ground level of the klystron gallery for penetration 1, 2 and the stairway. For the bent pentration-3, low enough dose rate is easily confirmed by the analytical calculation. (See section 7)

Horizontal cross sections of the MARS14 geometry at the underground beam line tunnel of the LCLS injector are shown in Figs. 4 and 5. Vertical cross sections are shown in Figs. 6 and 7 for the 2 slices of A-A' and B-B' of Fig. 5, respectively. To estimate dose attenuations through penetrations, detector cells were placed in the air region along the beam line tunnel and penetrations every 50 cm as shown in the figures. The soil region outside the concrete tunnel was defined as a black hole to terminate particle transport. Six iron targets (A~F) of 2 inch diameter sphere (see Fig. 8) were located in the tunnel, and electron beam of corresponding energies and directions were bombarded into the sphere surfaces as shown in Fig. 9.

For target-E and -F, a 2-step calculation was performed by dividing the geometry into 2 parts at around the 45 degree bending section of the tunnel. First, particles mainly produced backward from the target were stored separately in two files for hadrons (neutron) and EM-particles (electrons and photons) shown in Fig. 10. Second, two calculations starting with hadrons or EM-particles were performed from the 45 degree bending section as shown in Figs. 11 and 12, respectively. Finally, transmission profiles through penetrations were obtained up to the ground level for hadrons and EM-particles (mainly photons). For target-A and -B, no neutron contribution to the total dose because of low energy election beam.

Figs.13~18 show transmission profiles which were obtained by the MARS14 calculations. The calculated dose rates at the penetration exits in the klystron gallery floor are given in Table 3.

Table 3: Dose rates at the penetration exits in the ground level of klystron gallery floor calculated using the MARS14 Monte Carlo code.

		Target A 6.2MeV	Target B 6.2MeV	Target C 6.2MeV	Target D 6.2MeV	Target E 62MeV	Target F 135MeV
Penetration-1	[mrem/h]	2.1E+00	1.6E-01	7.3E-03	5.6E-03	2.5E-01	2.9E-01
Penetration-2	[mrem/h]	5.2E+00	1.3E+00	3.0E+02	1.7E+02	3.6E-01	2.0E-01
Stairway	[mrem/h]	3.1E-02	1.5E-02	4.1E-01	4.8E-01	2.3E-01	1.5E-01

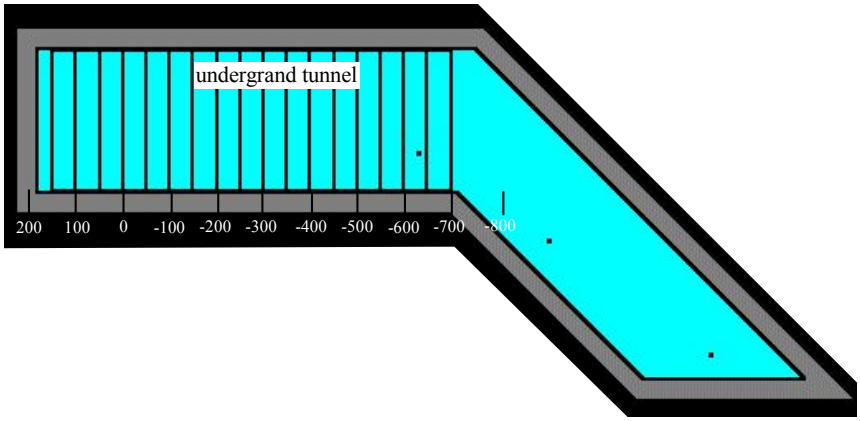

Fig.4: Horizontal cross section of the MARS14 geometry in underground beam line tunnel

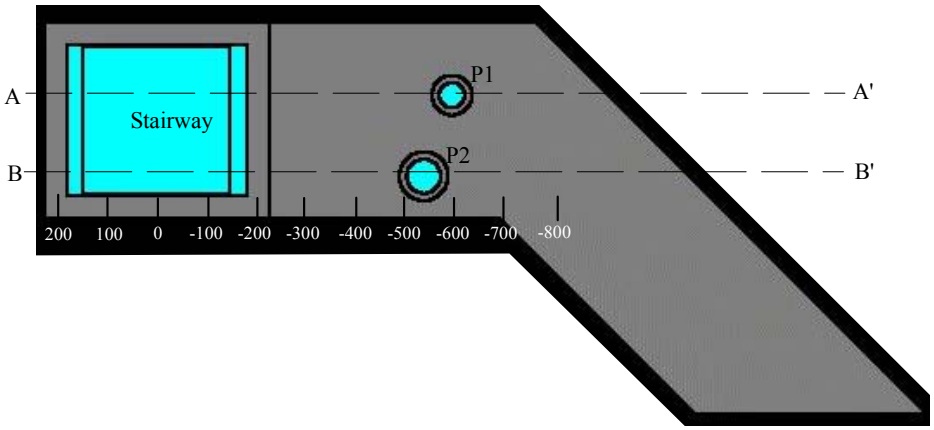

Fig.5: Horizontal cross section of the MARS14 geometry at the penetrations' mouths in underground beam line tunnel ceiling

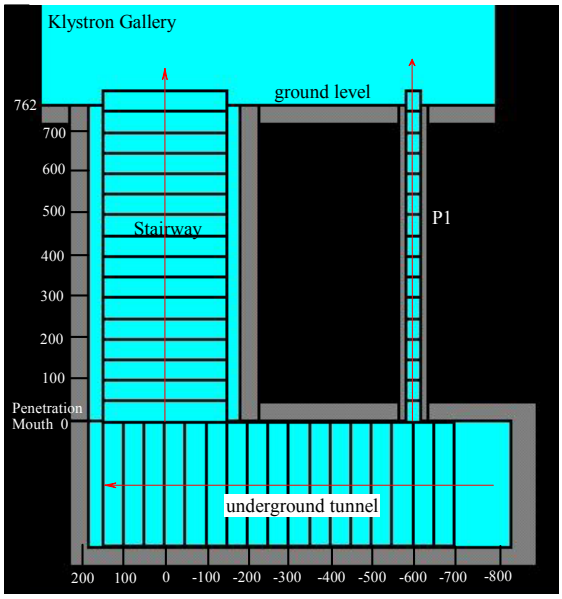

Fig. 6: Vertical cross section of the MARS14 geometry in penetration-1 for A-A' slice at Fig.5.

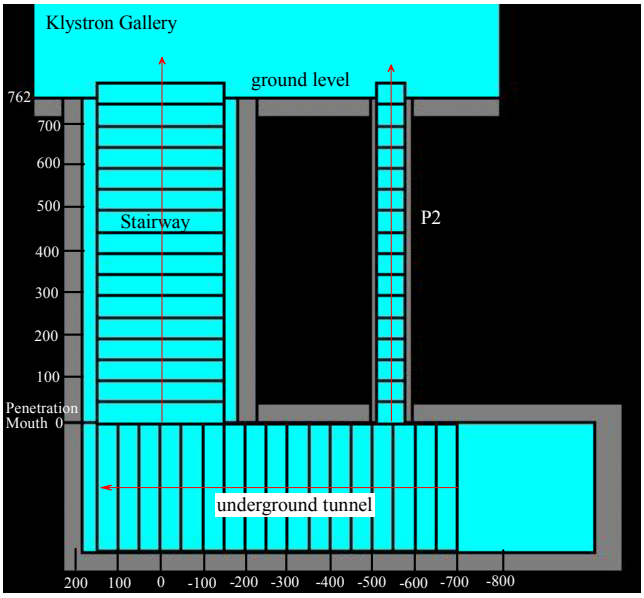

Fig. 7: Vertical cross section of the MARS14 geometry in penetration-2 for B-B' slice at Fig.5.

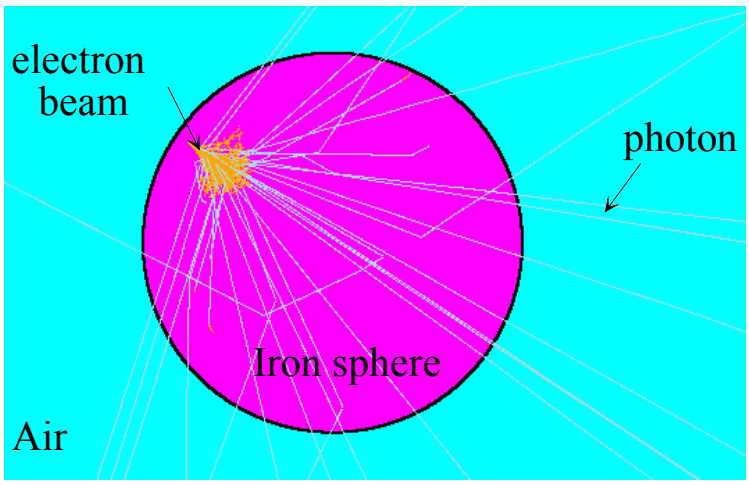

Fig.8: Track plots of 6.2 MeV electron bombardment on target-A (2 inch diameter sphere) in the MARS14 calculation.

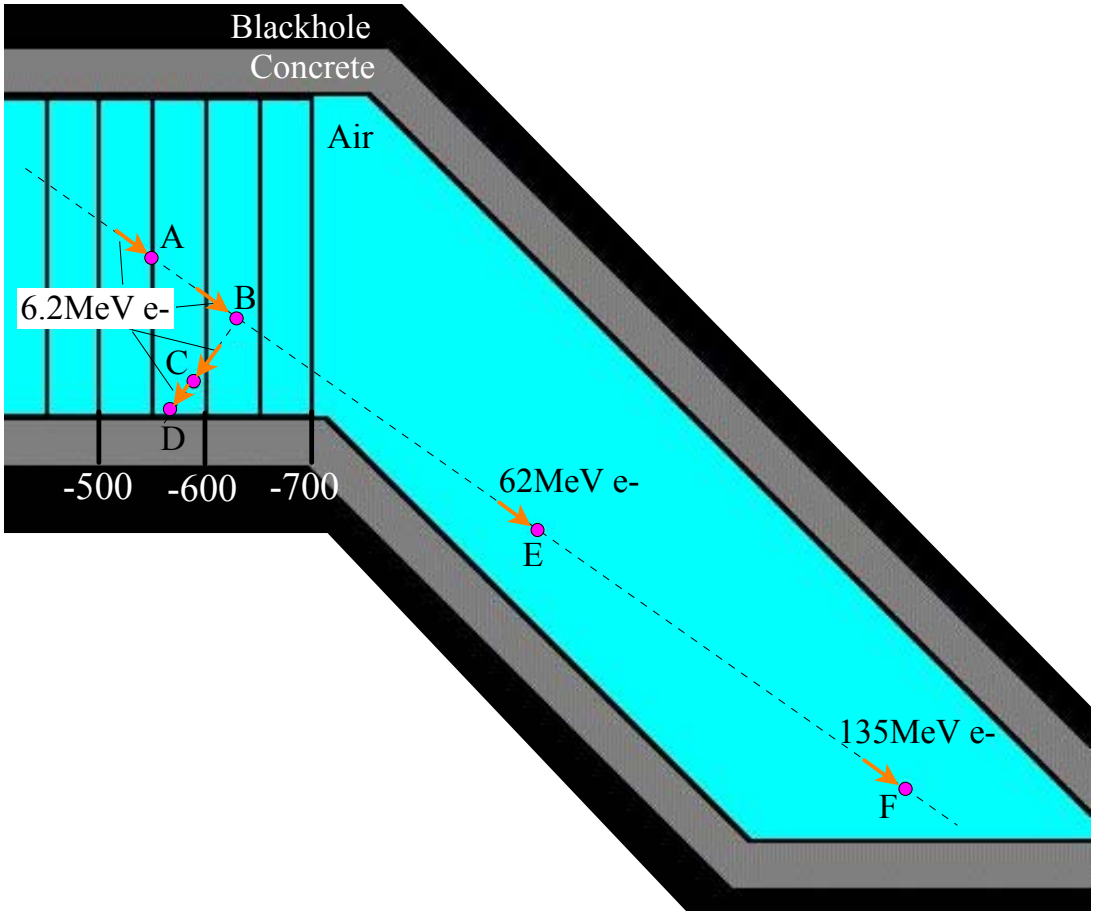

Fig.9: Target locations and electron beam in the tunnel in the MARS14 calculation.

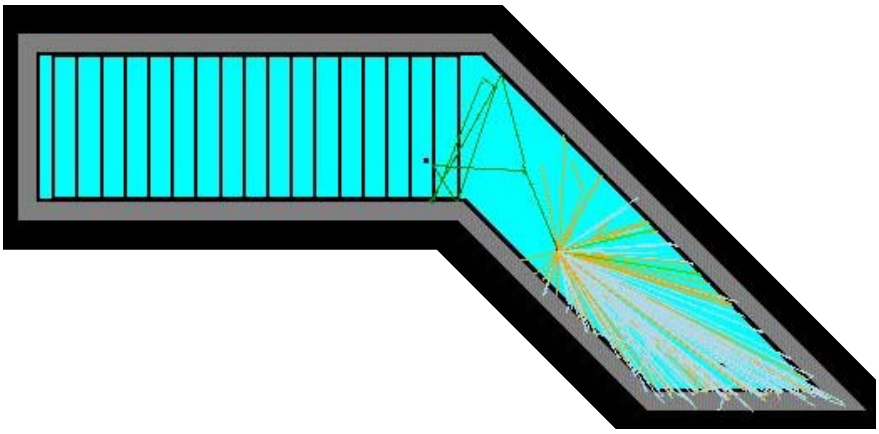

Fig.10: Track plots of 62 MeV electron bombardment on target-E (2 inch diameter sphere) in the MARS14 calculation

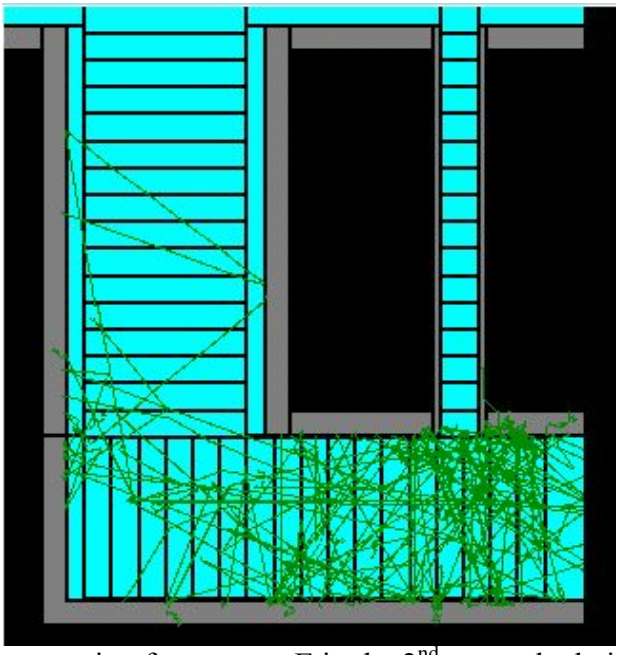

Fig.11: Neutron track plots coming from target E in the 2nd step calculation by the MARS14 code

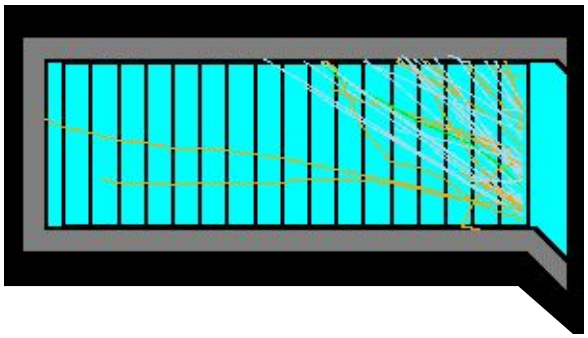

Fig.12: Track plots of electrons and photons from target E in the 2nd step calculation by the MARS14

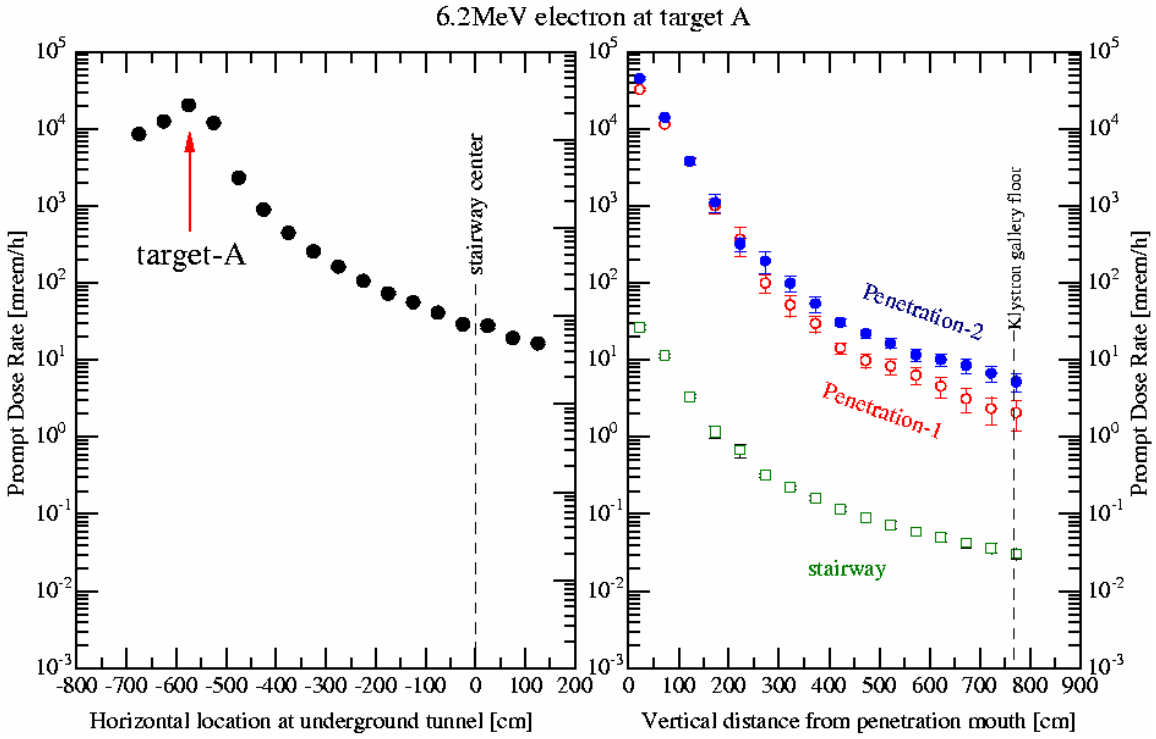

Fig.13: Transmission curves of dose rate through underground tunnel and penetrations in the case of 6.2 MeV on target-A calculated using the MARS14 code.

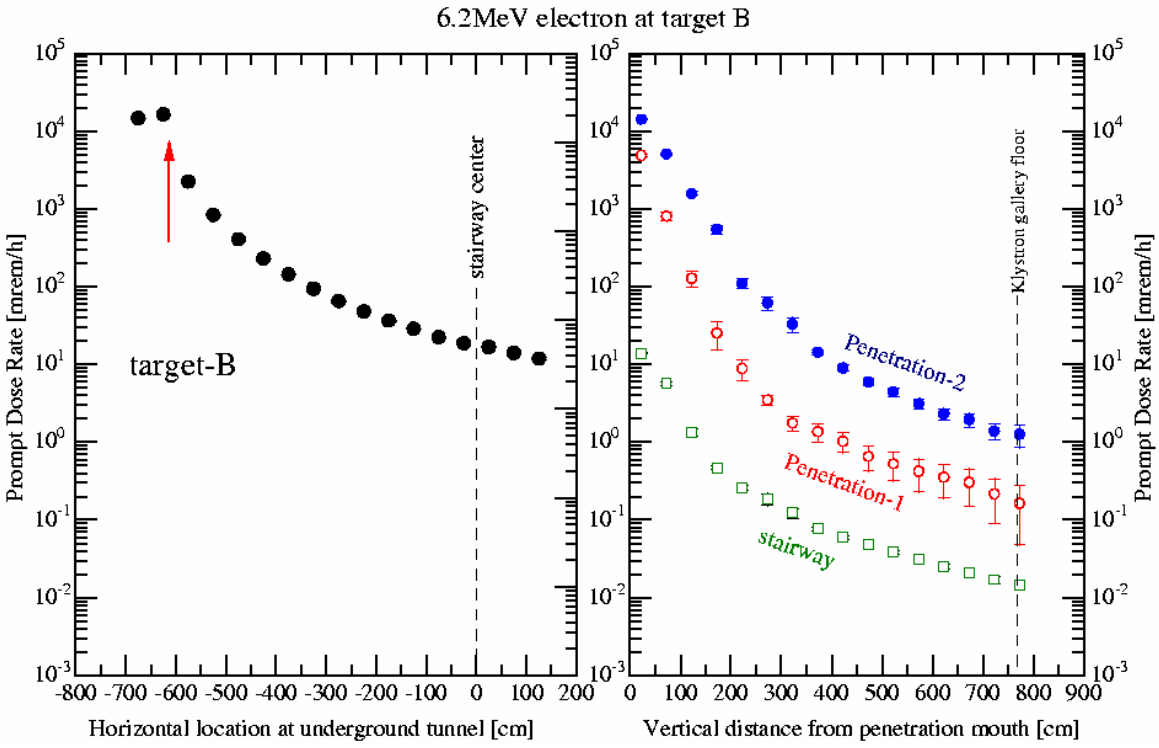

Fig. 14: Transmission curves of dose rate through underground tunnel and penetrations in the case of 6.2 MeV on target-B calculated using the MARS14 code.

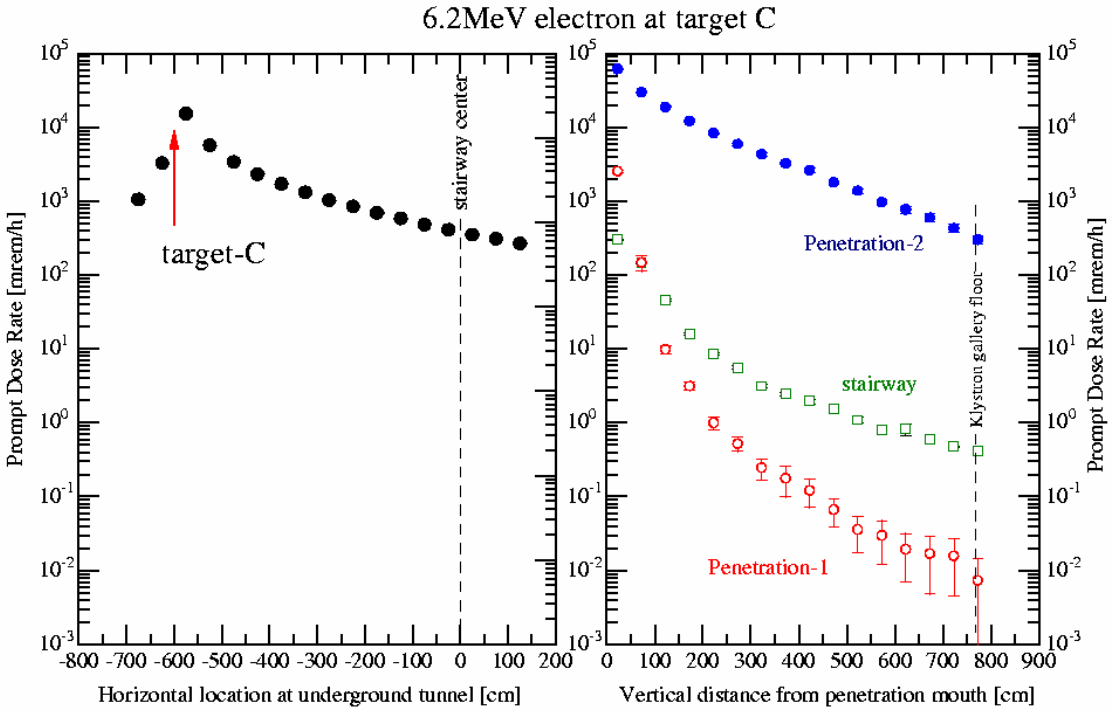

Fig. 15: Transmission curves of dose rate through underground tunnel and penetrations in the case of 6.2 MeV on target-C calculated using the MARS14 code.

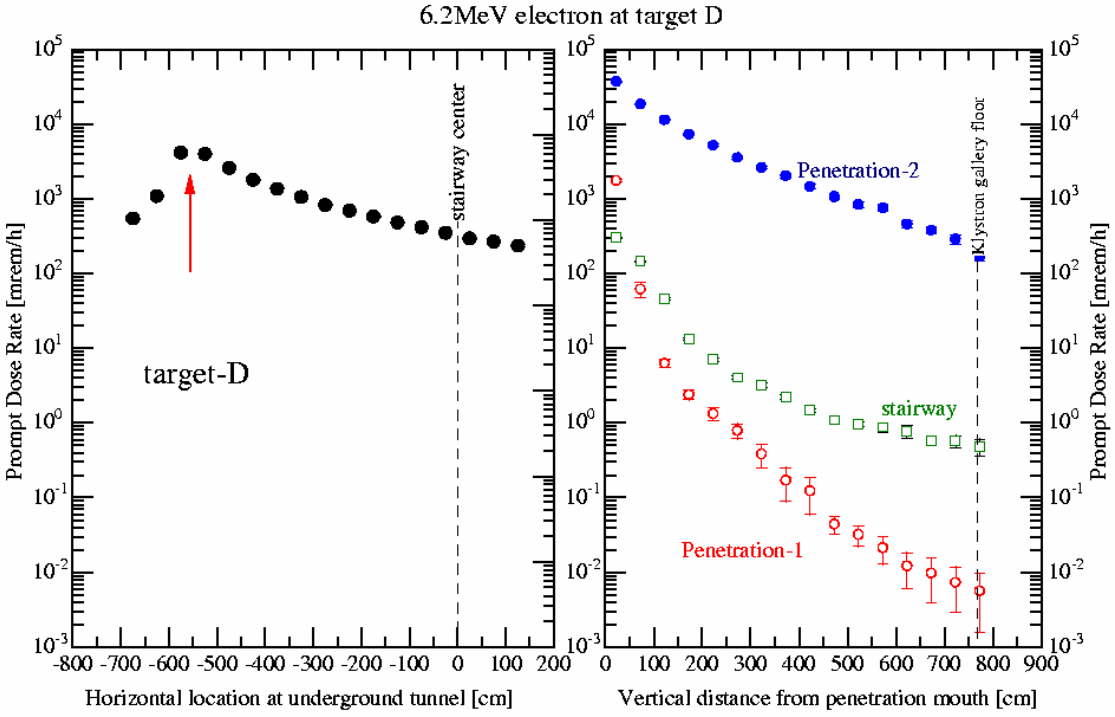

Fig. 16: Transmission curves of dose rate through underground tunnel and penetrations in the case of 6.2 MeV on target-D calculated using the MARS14 code.

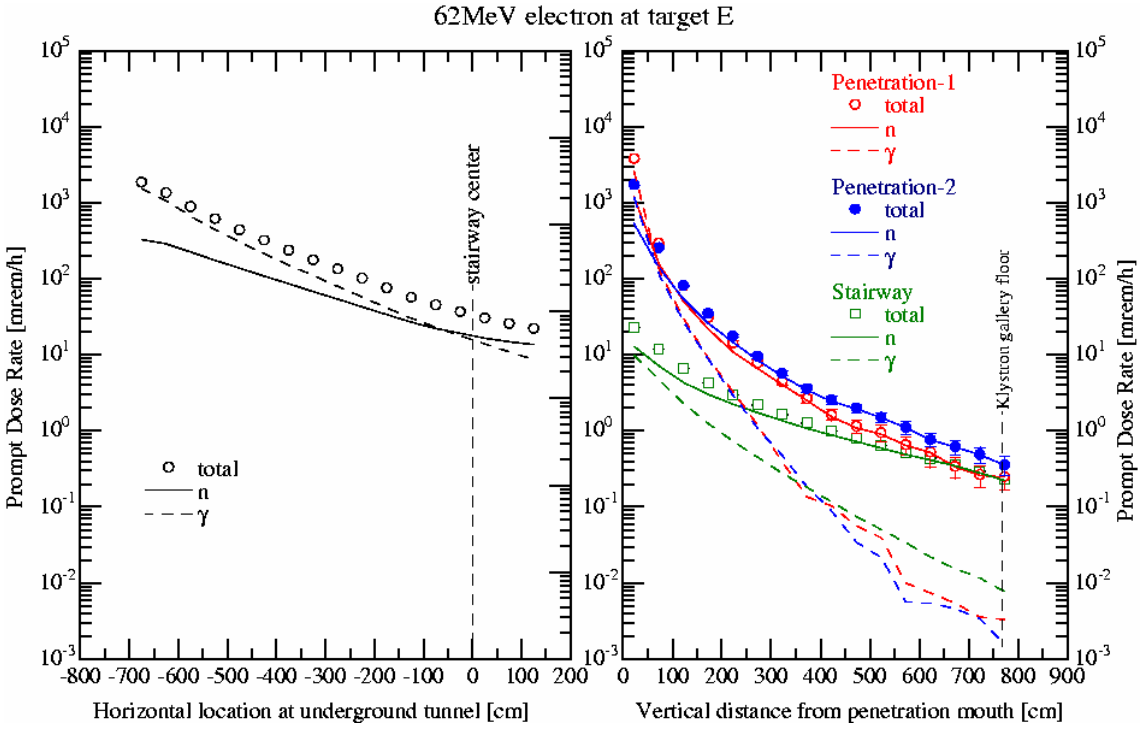

Fig.17: Transmission curves of dose rate through underground tunnel and penetrations in the case of 62 MeV on target-E calculated using the MARS14 code.

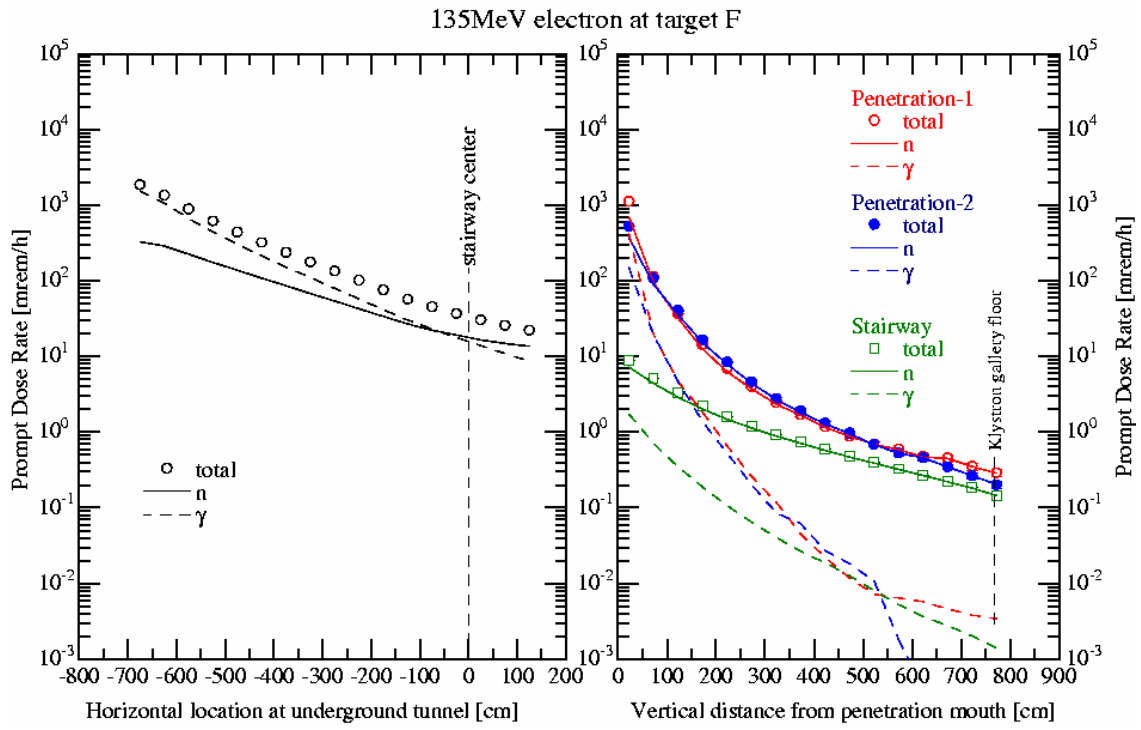

Fig.18: Transmission curves of dose rate through underground tunnel and penetrations in the case of 135 MeV on target-F calculated using the MARS14 code.

5) Comparisons between MARS14 and FLUKA calculations

Calculation through the stairway to ground level in the case of 6.2 MeV electrons bombarded into target C was also performed using the FLUKA Monte Carlo code [2,3]. Fig.19 shows a vertical two-dimensional distribution of dose rate at the beam line tunnel and the stairway. In Fig.20, the attenuation profile of dose rate through the stairway by FLUKA is compared with the results by the MARS14 code.

Although discrepancy between two calculations can be found around the penetration mouth, generally these two results agreed well especially at the klystron gallery floor. Therefore, these two simulations using Monte Carlo method are considered to be reliable.

This FLUKA calculation also indicates that the dose rates are reduced by a factor of two at one foot away from the stairway at the klystron gallery floor. (See Fig. 19)

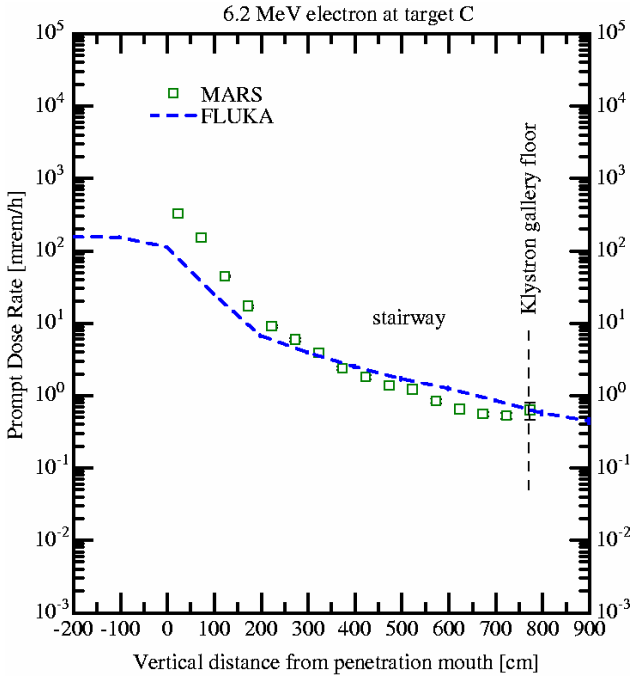

Fig. 20: Comparison of dose rate attenuation through the stairway between MARS and FLUKA

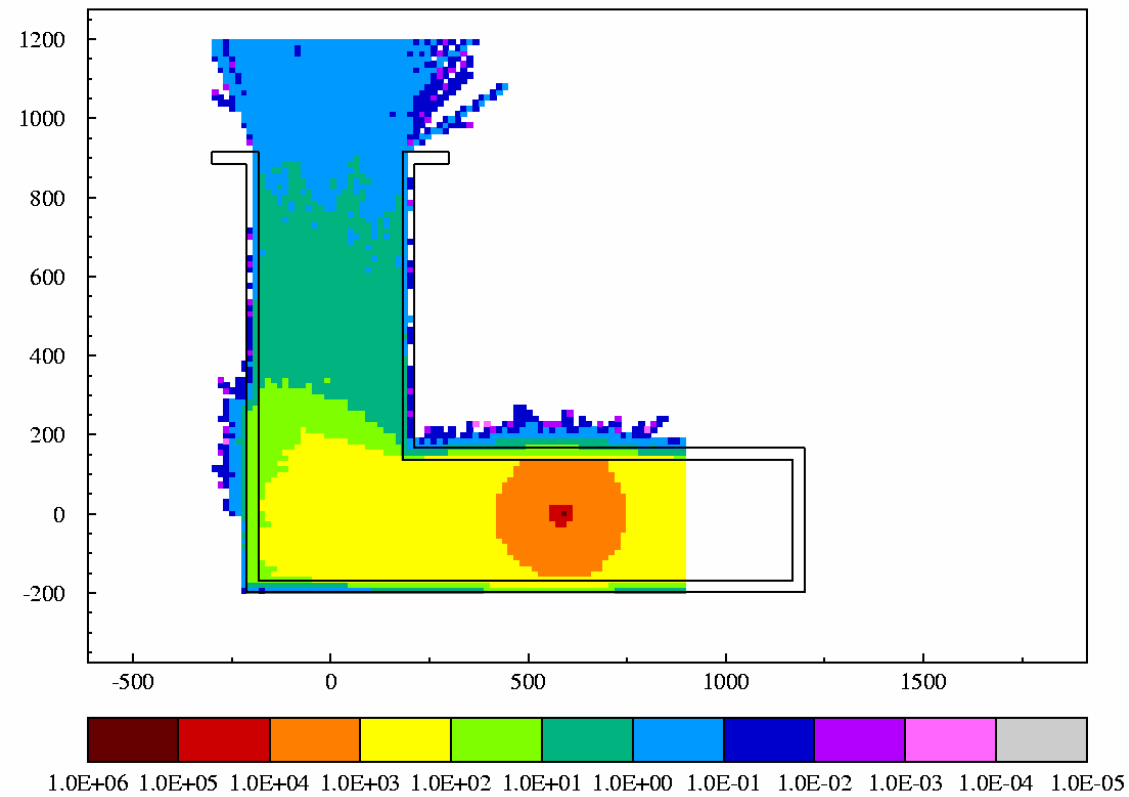

Fig.19: Two-dimensional distribution of dose rate (mrem/h) for 6.2 MeV electron bombardment into the target-C calculated using the FLUKA Monte Carlo code

6) Estimation of dose rates in operation

Dose rates in operation at the ground level exits of penetration-1, -2 and the stairway were estimated using the MARS14 results. Table 4 gives the maximum dose rates at each exit considering the dark current which occurs the combination of either A, E, F or B, E, F. There is no dark current at target C and D. Maximum dose rates were calculated by summation of the higher case of dark current combination and maximum dose rate by beam. The dose rates for 55.8 and 72.9 MeV cases were estimated by scaling using 62 and 135 MeV results, respectively.

Table 4: Beam losses and dose rates on the penetration without shielding (Dose rate = mrem/hr)

Target	Beam parameter	Laser Penetration 1	Unused Penetration 2	Stairway
A	Dark current 6.2 MeV, 0.744 W	Dark current 2.1, A or B	Dark current 5.2, A or B	Dark current 0.031, A or B
	Beam 6.2 MeV, 0.744 W	2.1	5.2	0.031
B	Dark current 6.2 MeV, 0.744 W	Dark current 0.16, A or B	Dark current 1.3, A or B	Dark current 0.015, A or B
	Beam 6.2 MeV, 0.744 W	0.16	1.3	0.015
C	Dark current	N/A	N/A	N/A
	Beam 6.2 MeV, 0.744 W	0.0073	300	0.41
D	Dark current	N/A	N/A	N/A
	Beam 6.2 MeV, 0.744 W	0.0056	170	0.48
E	Dark current 55.8 MeV, 1.06 W	Dark current 0.036	Dark current 0.051	Dark current 0.033
	Beam 62 MeV, 7.44 W	0.25	0.36	0.23
F	Dark current 72.9 MeV, 1.39 W	Dark current 0.025	Dark current 0.017	Dark current 0.013
	Beam 135 MeV, 16.2 W	0.29	0.20	0.15
Maximum	Dark current	2.2	5.3	0.08
	Beam	2.1	300	0.48
	Total	4.3	305	0.56

- Dark current losses happen at the combination of either (A, E, F) or (B, E, F) at the same time.
- Beam loss happens at one of these points at the same time.
- Only gamma radiation is produced from Target A, B, C, and D.
- Neutron is dominant for Target E and F.

7) Analytical calculation and comparison with MARS14

7-1) Source term at penetration mouth

In the case of 6.2 MeV electron injection, the angular distribution for 8 MeV electrons as shown in Fig. 21 [5] was used to estimate source terms at the center of the penetration mouth. On the other hand, in the case of higher energy, dose rates were estimated with using the SHIELD11 code [6].

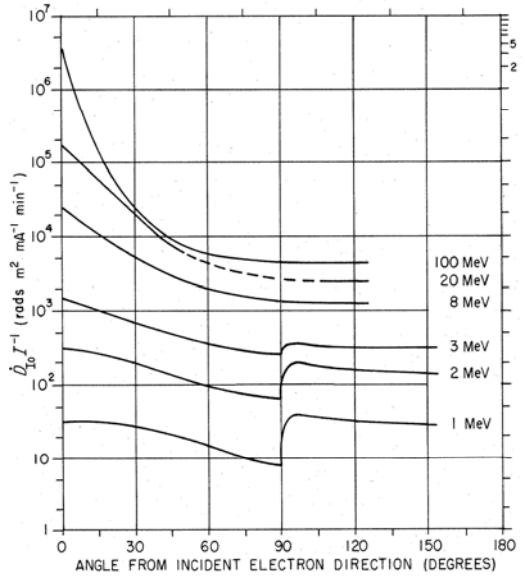

Fig.21: Angular distribution of emitted X rays from High-Z targets [5]

7-2) Transmission curve in penetration

To estimate the attenuation through penetrations from the source term, transmission curves shown in Figs. 22 and 23 from Ref.[7] were used for the 1st leg and the 2nd leg, respectively. In this work, the curves for point off axis were used for the 1st leg calculations. Curve b and c in Fig. 23 were used for attenuations of neutrons and photons, respectively, for the 2nd leg, which is empirically confirmed with experiments and simulations [8]. Although the stairway is the first leg in the cases for target A~D, it is considered to be the 2nd leg because of the large distances from the targets to the penetration mouth (stairway mouth).

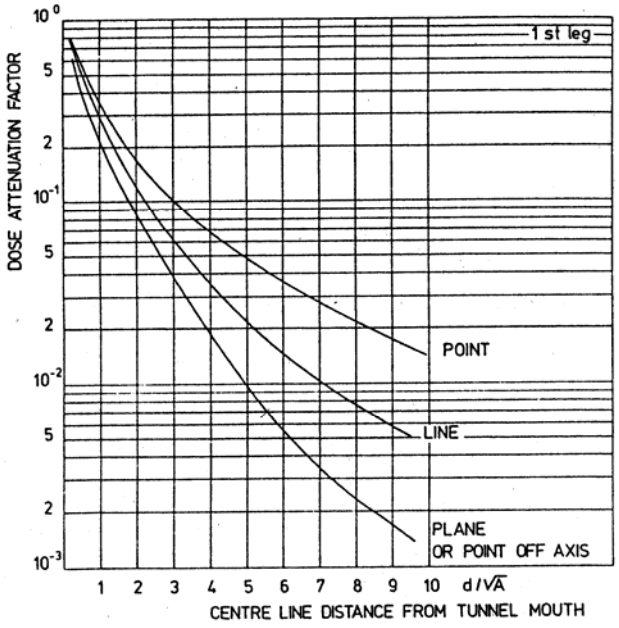

Fig.22: Transmission curves for 1st leg [7]

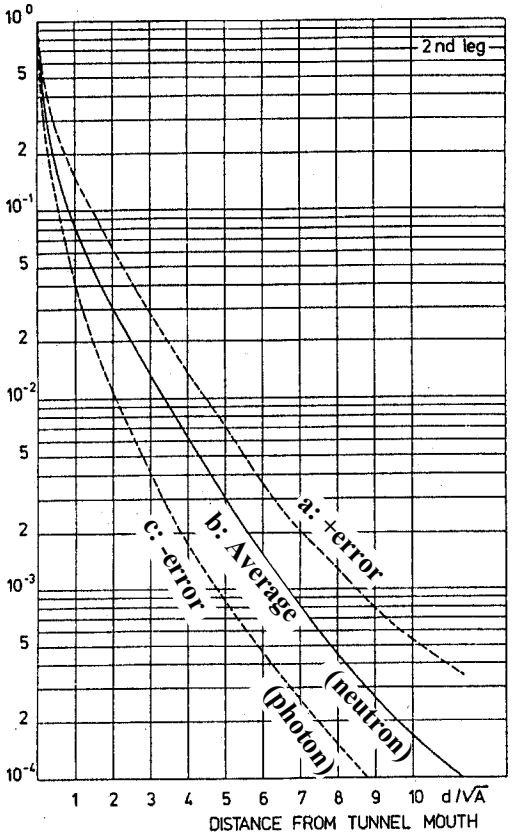

Fig.23: Transmission curves for 2nd leg [7].

7-3) Comparisons between MARS14 and analytical method

Dose rates were compared between MARS results and analytical method at the penetration exits in the ground level and mouths in the tunnel ceiling as given in Table 5 and 6, respectively. Source terms of the analytical method for the stairway are shown in left figures of Figs.24, 26, 28, 30 and 32. Attenuations through penetration-1, -2 and the stairway are shown in right of those figures. Sketches of the analytical calculation process for various targets are shown in Figs.25, 27, 29, 31 and 33. In the case that the stairway is located at backward of beam direction such as target A and B, source terms expressed with $1/r^2$ are larger than those of the MARS14, on the other hand, they agree well in the forward case such as C and D.

Transmission curves for 1st and 2nd legs are compared relatively with those obtained by the MARS14 as shown in Fig.34. Generally attenuations for the 1st leg by the MARS14 are steeper than the analytical curves in the beginning of penetrations, but become to agree in the deeper region. On the other hand, attenuation for penetrations-2 from target-C by the MARS14 was much slower than the analytical curve of the 1st leg for off axis as shown in the left figure of Fig. 34 because the secondary particles produced at target-C and -D can be directly transmitted to the middle of penetration-2. For 2nd leg, generally analytical curves are slower that those by the MARS14 as shown in the right of Fig. 34.

Table 5: Comparisons of dose rates at penetration exits between the MARS14 and analytical method.

			Target A 6.2MeV	Target B 6.2MeV	Target C 6.2MeV	Target D 6.2MeV	Target E 62MeV	Target F 135MeV
Pene-1	MARS	[mrem/h]	2.1E+00	1.6E-01	7.3E-03	5.6E-03	2.5E-01	2.9E-01
	Analytic	[mrem/h]	3.4E-01	2.4E-01	1.8E-01	1.5E-01	6.1E-02	3.9E-02
	Analy/MARS	ratio	**0.16**	**1.5**	**24.7**	**26.8**	**0.24**	**0.13**
Pene-2	MARS	[mrem/h]	5.2E+00	1.3E+00	3.0E+02	1.7E+02	3.6E-01	2.0E-01
	Analytic	[mrem/h]	1.6E+00	1.3E+00	2.1E+00	2.0E+00	5.7E-03	2.6E-03
	Analy/MARS	ratio	**0.31**	**1.0**	**0.007**	**0.012**	**0.016**	**0.013**
Stairway	MARS	[mrem/h]	3.1E-02	1.5E-02	4.1E-01	4.8E-01	2.3E-01	1.5E-01
	Analytic	[mrem/h]	2.1E+00	1.7E+00	2.7E+00	2.8E+00	9.4E-01	4.1E-01
	Analy/MARS	ratio	**68.6**	**113**	**6.6**	**5.8**	**4.1**	**2.8**
Pene-3	Analytic	[mrem/h]	-	1.4E-05	-	-	1.1E-05	4.8E-06

Table 6: Comparisons of dose at penetration mouths between the MARS14 and analytical method

			Target A 6.2MeV	Target B 6.2MeV	Target C 6.2MeV	Target D 6.2MeV	Target E 62MeV	Target F 135MeV
Pene-1	MARS	[mrem/h]	3.2E+04	4.9E+03	2.5E+03	1.8E+03	3.8E+03	1.1E+03
	Analytic	[mrem/h]	2.8E+03	2.0E+03	1.5E+03	1.2E+03	5.1E+02	3.3E+02
	Analy/MARS	ratio	**0.087**	**0.41**	**0.58**	**0.70**	**0.13**	**0.29**
Pene-2	MARS	[mrem/h]	4.5E+04	1.4E+04	6.1E+04	3.7E+04	1.7E+03	5.2E+02
	Analytic	[mrem/h]	3.1E+03	2.5E+03	4.0E+03	3.8E+03	6.2E+00	1.7E+02
	Analy/MARS	ratio	**0.068**	**0.17**	**0.065**	**0.10**	**0.0036**	**0.33**
Stairway	MARS	[mrem/h]	2.7E+01	1.4E+01	3.0E+02	3.0E+02	2.3E+01	9.0E+00
	Analytic	[mrem/h]	2.3E+02	1.9E+02	3.0E+02	3.1E+02	1.2E+01	3.3E+01
	Analy/MARS	ratio	**8.6**	**13.6**	**1.0**	**1.0**	**0.52**	**3.7**

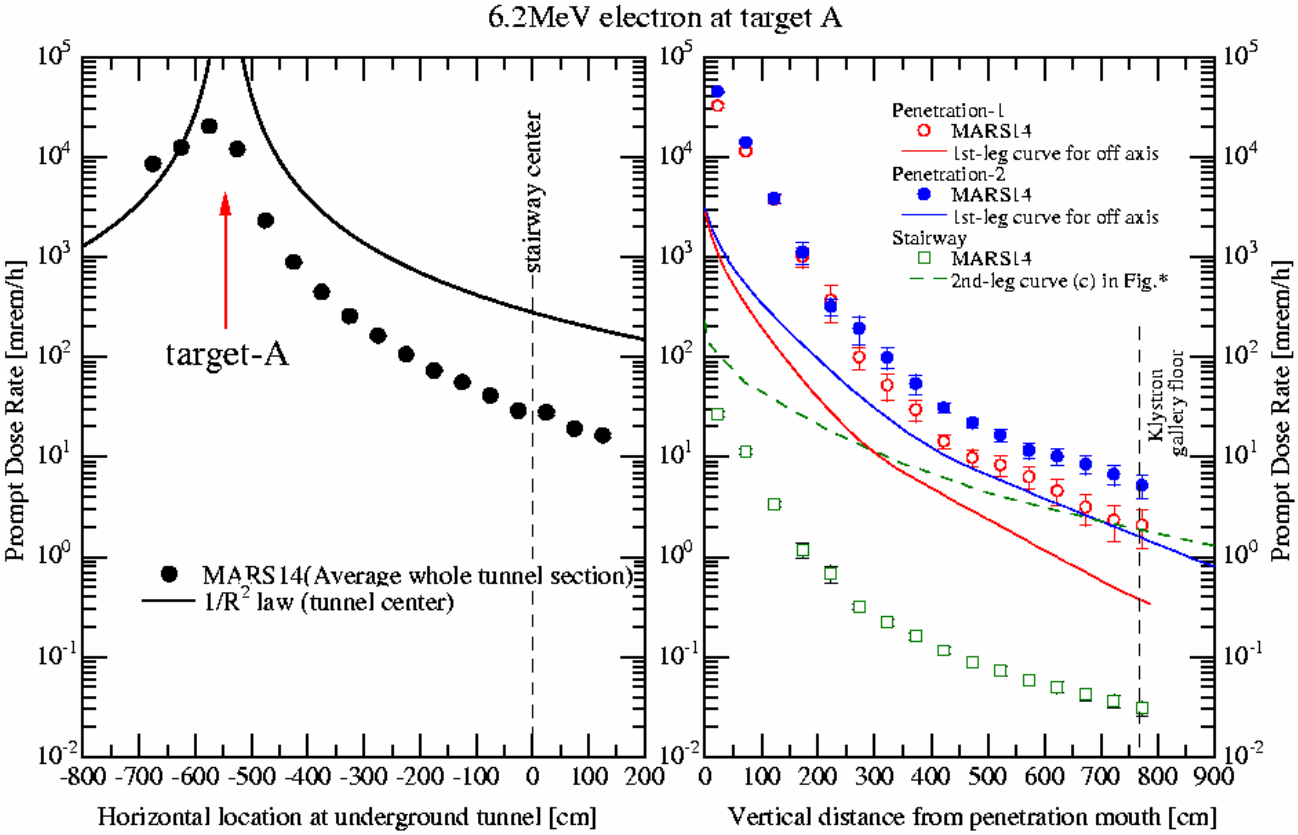

Fig.24: Dose rate attenuations from analytical calculation for target A compared with the MARS14

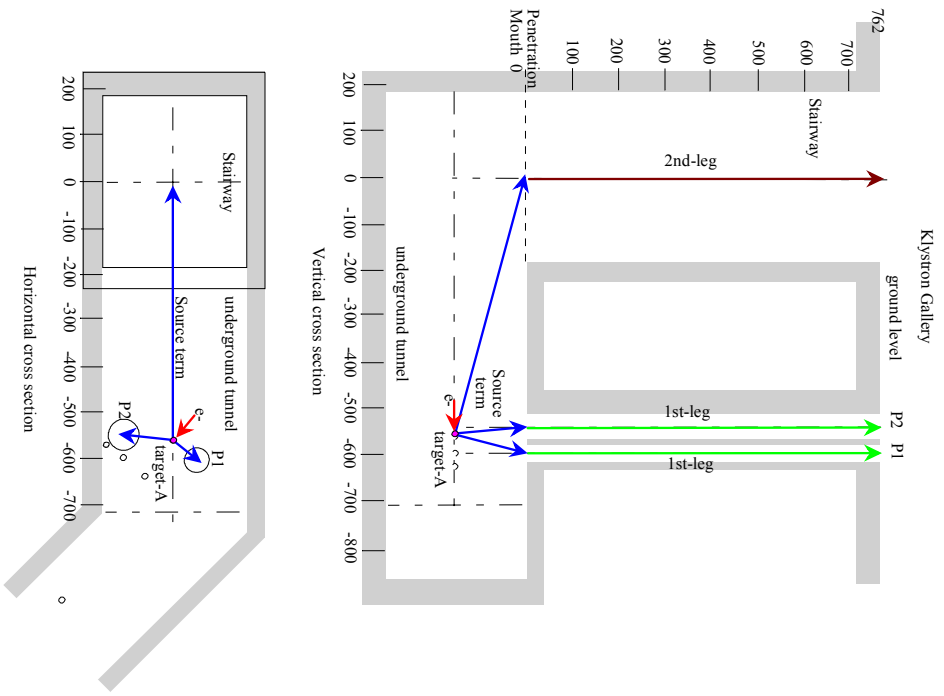

Fig.25: A sketch of the analytical calculation process for target A.

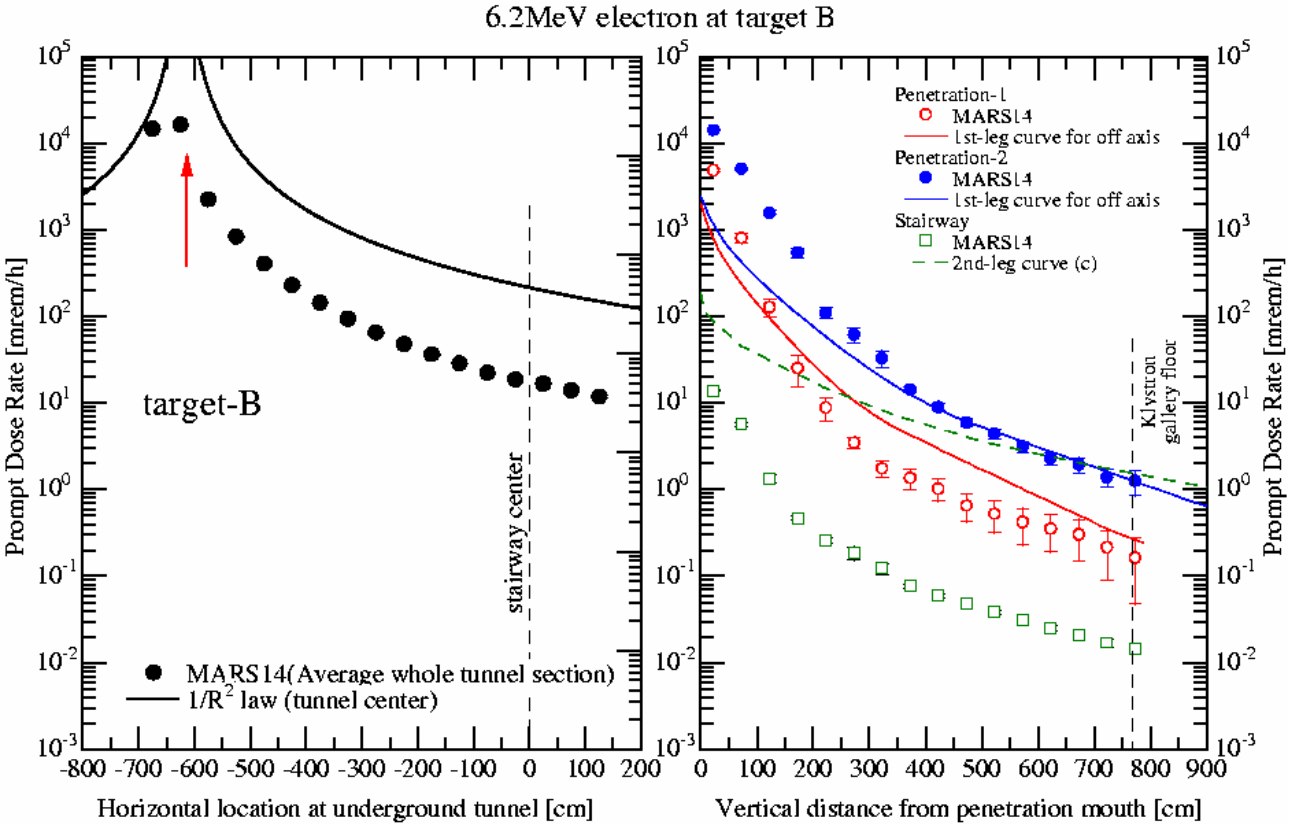

Fig.26: Dose rate attenuations from analytical calculation for target B compared with the MARS14

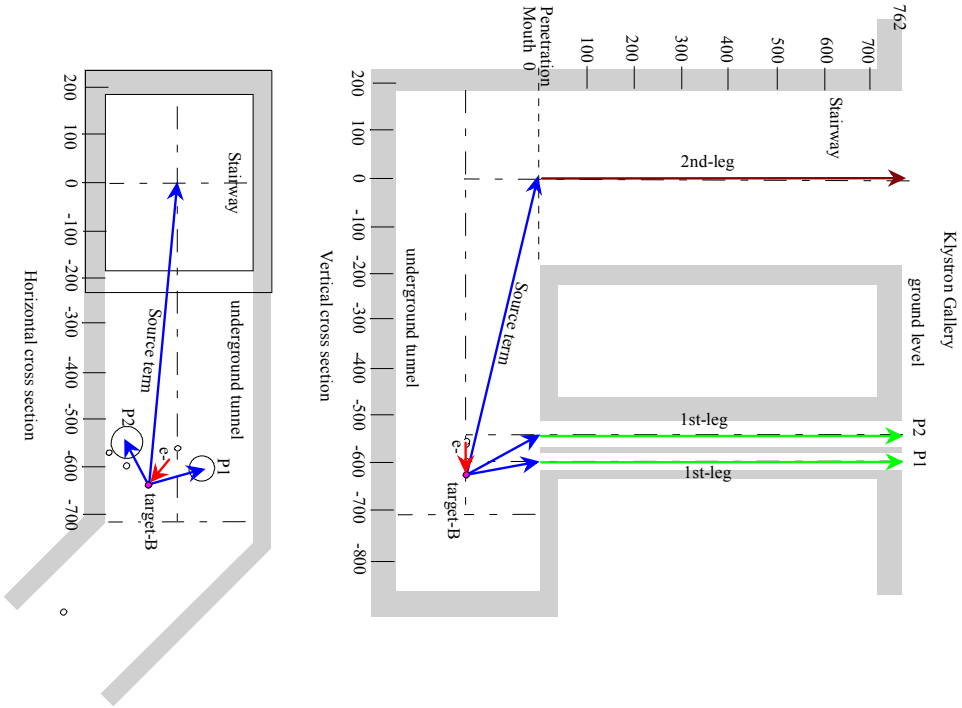

Fig.27: A sketch of the analytical calculation process for target B.

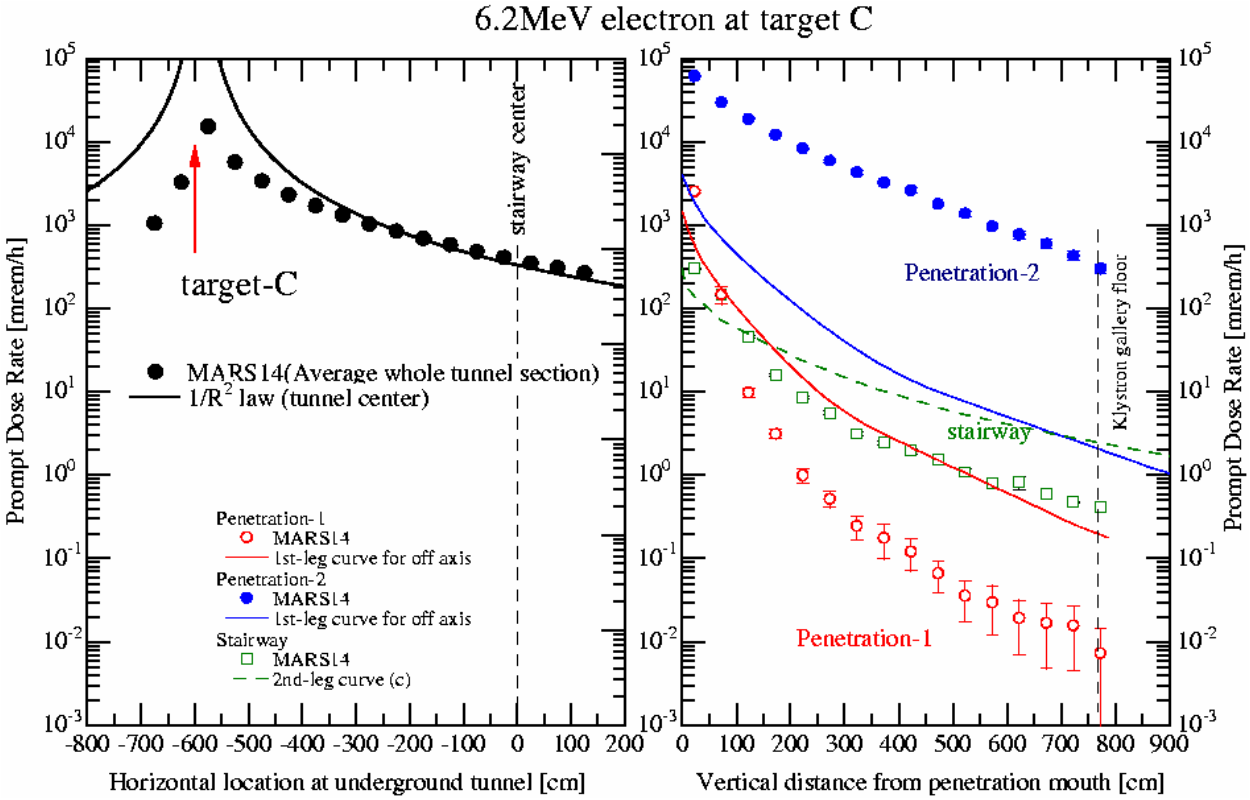

Fig.28: Dose rate attenuations from analytical calculation for target C compared with the MARS14

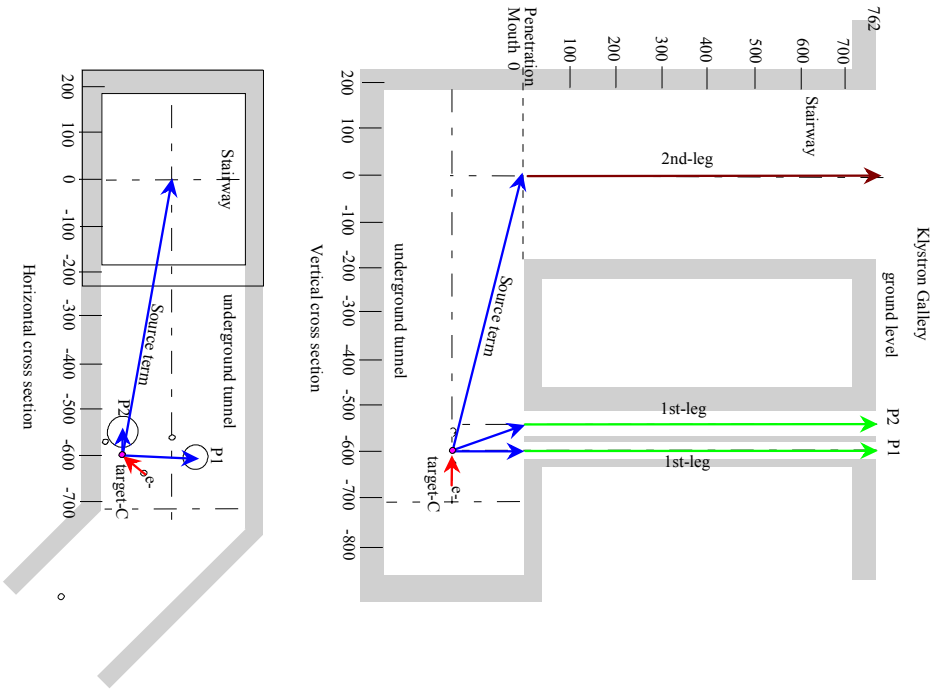

Fig.29: A sketch of the analytical calculation process for target C.

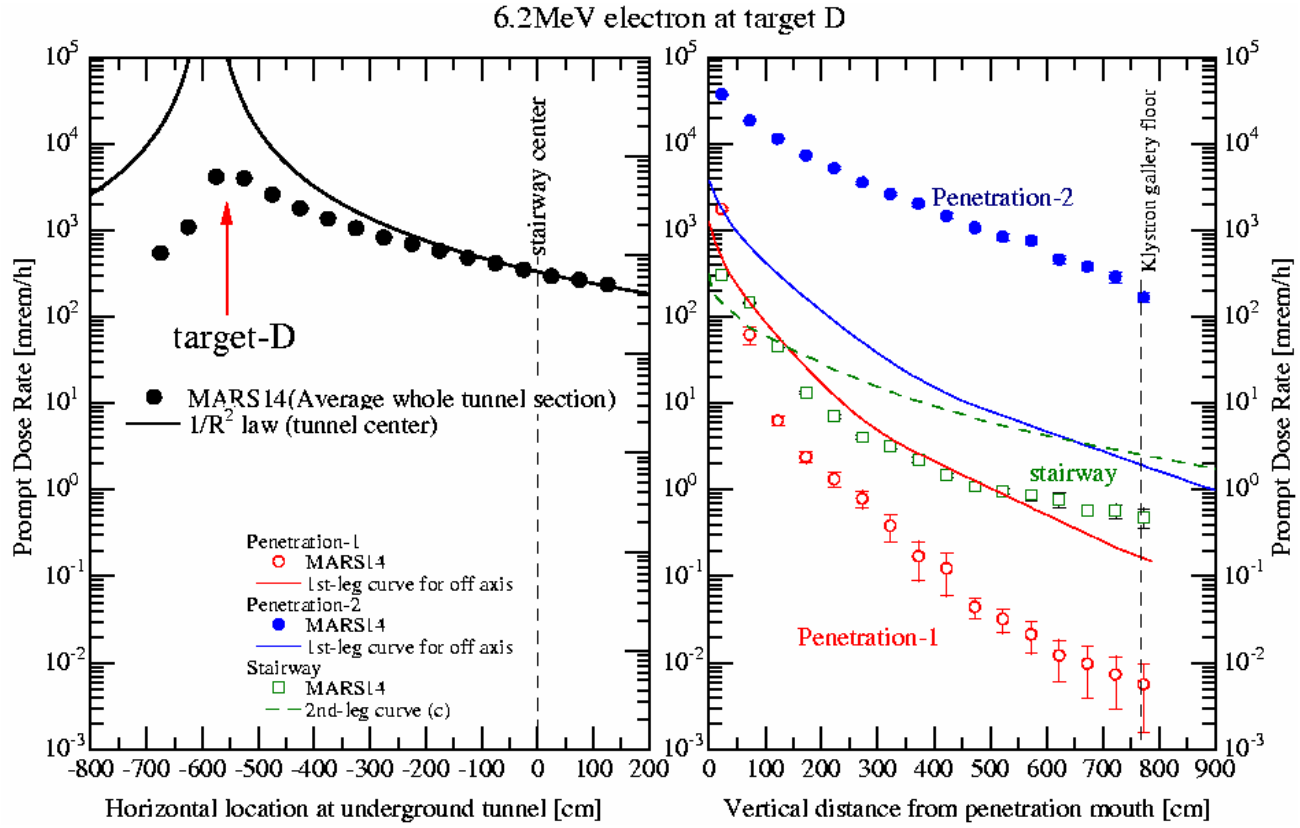

Fig.30: Dose rate attenuations from analytical calculation for target D compared with the MARS14

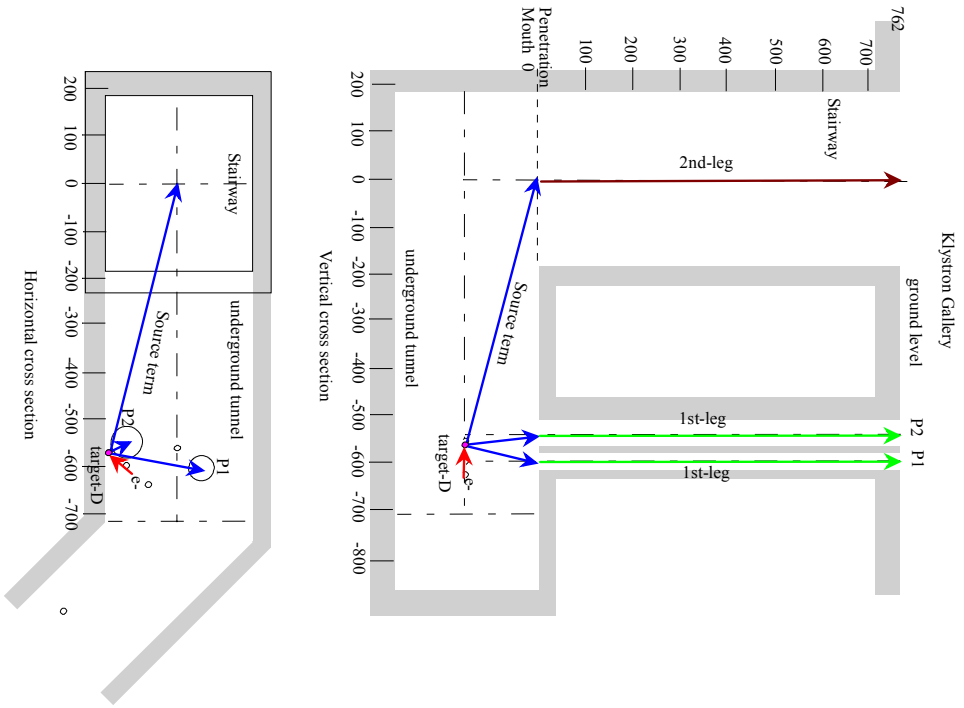

Fig.31: A sketch of the analytical calculation process for target D.

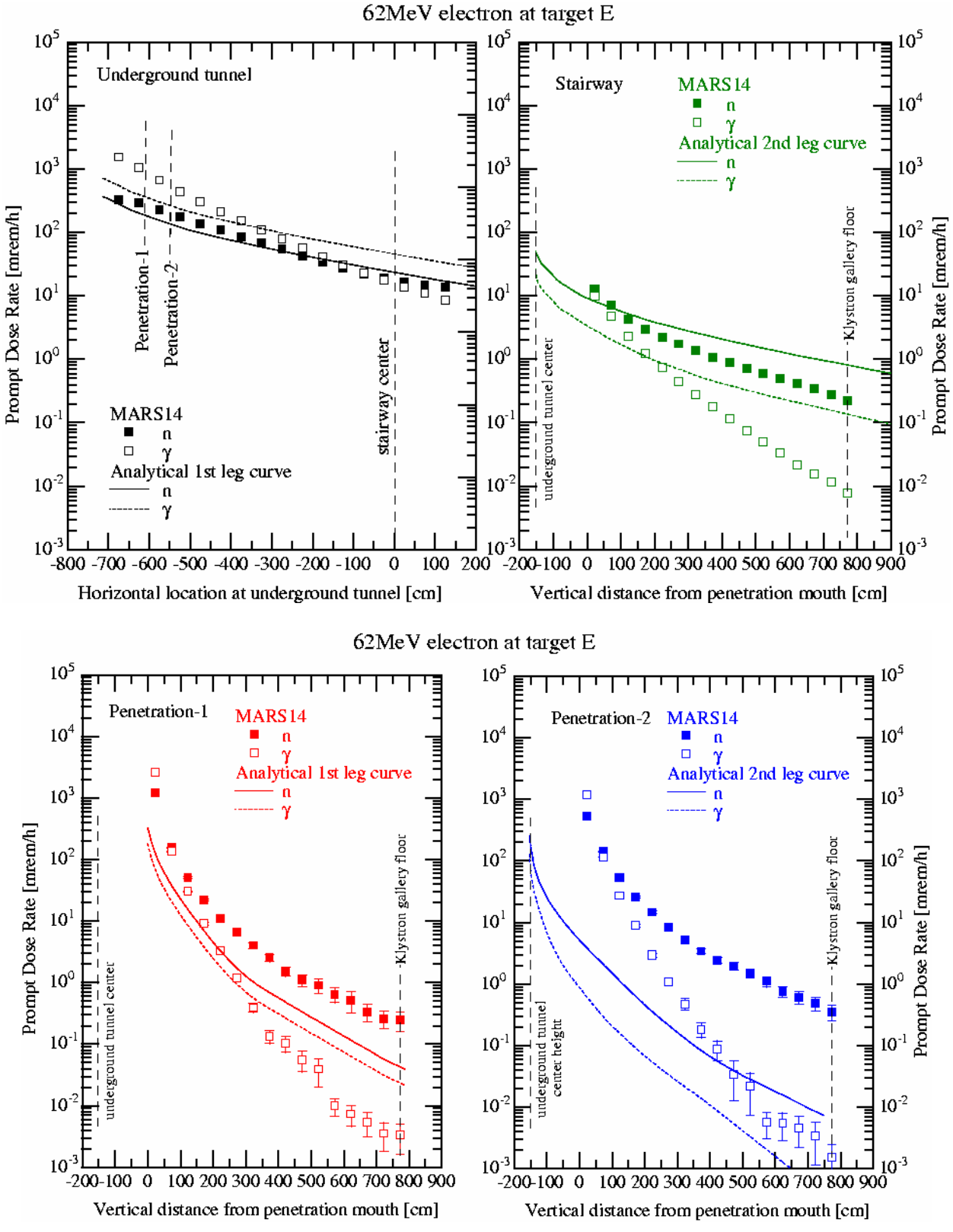

Fig. 32: Dose rate attenuations from analytical calculation for target E compared with the MARS14 (Those for target-F are similar results.)

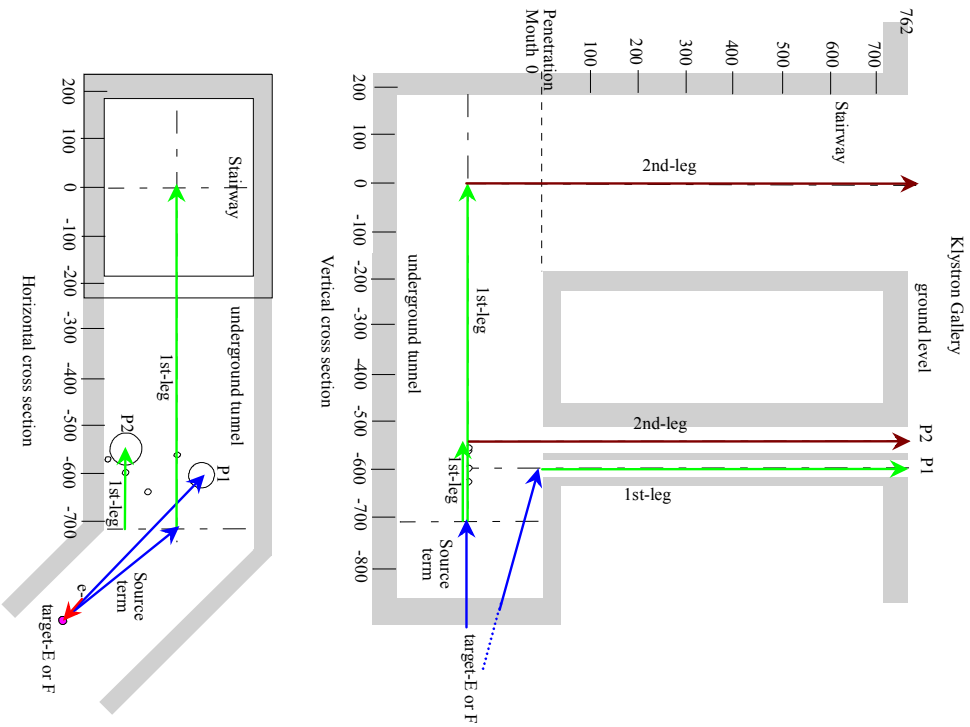

Fig.33: A sketch of the analytical calculation process for target E or F.

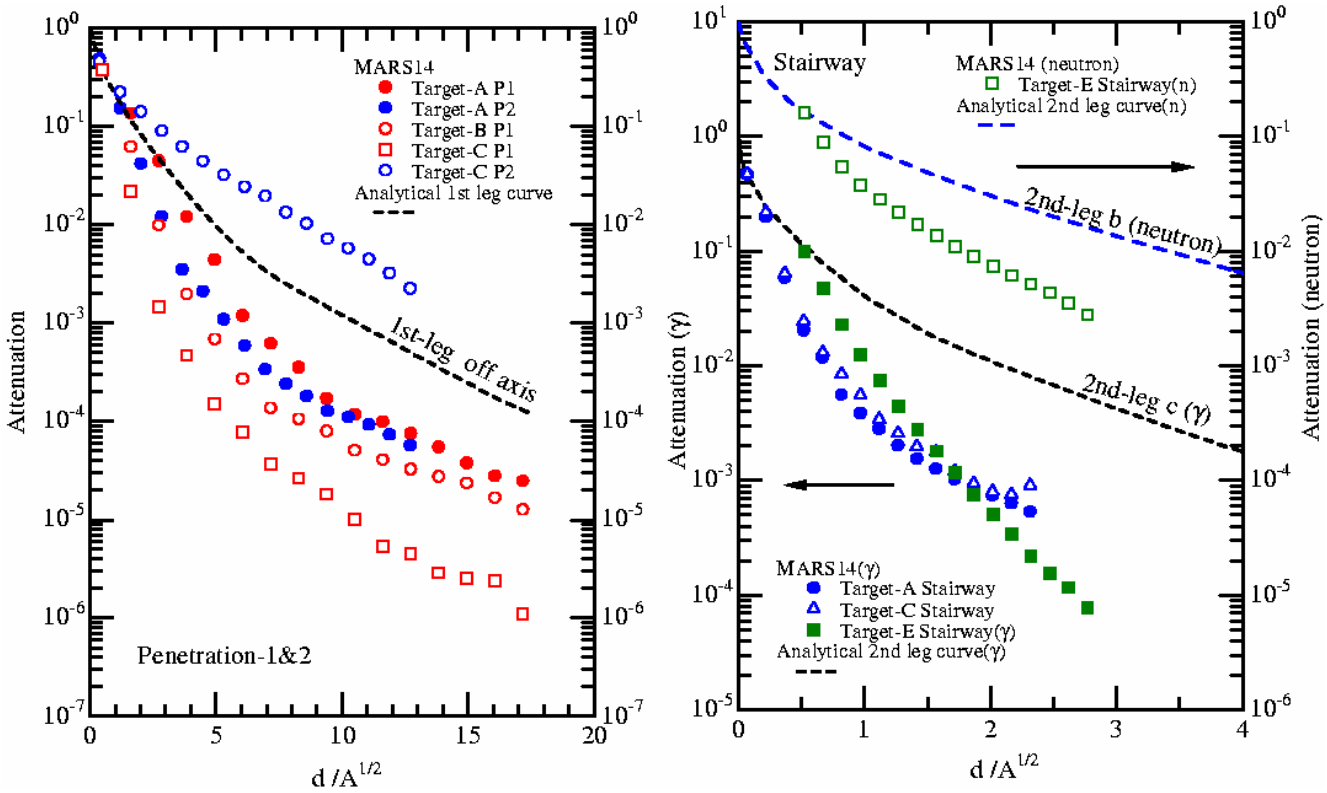

Fig.34: Transmission curves in the 1st and the 2nd legs of penetration in Ref.[7] compared with those obtained by the MARS14 calculation normalized at the beginning of penetration

REFERENCES

[1] N. V. Mokhov, "The Mars Code System User's Guide", Fermilab-FN-628 (1995); N. V. Mokhov and O.E.Krivosheev,"MARS Code Status",Fermilab-Conf-00/181(2000);http://www-ap.fnal.gov/MARS.

[2] A. Fasso, A. Ferrari, P. R. Sala, *Electron-Photon transport in FLUKA*: status, invited talk in the Proceedings of the Monte Carlo 2000 Conference, Lisbon, October 23-26 2000, A. Kling, F. Barao, M. Nakagawa, L. Tavora, P. Vaz, eds., Springer-Verlag Berlin, p.159-164 (2001)

[3] A. Fasso, A. Ferrari, J. Ranft, and P. R. Sala, FLUKA: *Status and Prospective for Hadronic Applications*, invited talk in the Proceedings of the Monte Carlo 2000 Conference, Lisbon, October 23-26 2000, A. Kling, F. Barao, M. Nakagawa, L. Tavora, P. Vaz, eds., Springer-Verlag Berlin, p.955-960 (2001)

[4] D. H. Dowell, "Estimates of Linac Dark Current Losses at Sector 20," March 3, 2003, Memo to X. S. Mao and A. A. Prinz.

[5] "Radiation Protection Design Guidelines for 0.1-100 MeV Particle Accelerator Facilities", NCRP report No.51, National Council on Radiation and Measurements (1977)

[6] W. R. Nelson, and T. Jenkins, "SHELD11 Shielding Code", Stanford Linear Accelerator Center, Stanford, CA 94087 (1989)

[7] Ralph H. Thomas et al., "Radiological Safety Aspects of the Operation of Protection Accelerators", Technical Reports Series No.283, International Atomic Energy Agency, Vienna, (1988).

[8] Albert Fasso, Private communication.